

A machine learning framework for the prediction of chromatin folding in *Drosophila* using epigenetic features

Michal B. Rozenwald^{Corresp., 1}, Aleksandra A. Galitsyna², Grigory V. Sapunov^{1,3}, Ekaterina E. Khrameeva², Mikhail S. Gelfand^{Corresp., 2, 4}

¹ Faculty of Computer Science, National Research University Higher School of Economics, Moscow, Russia

² Center of Life Sciences, Skolkovo Institute of Science and Technology, Moscow, Russia

³ Intento, Inc, Berkeley, CA, USA

⁴ A.A. Kharkevich Institute for Information Transmission Problems, RAS, Moscow, Russia

Corresponding Authors: Michal B. Rozenwald, Mikhail S. Gelfand
Email address: mbrozenvald@edu.hse.ru, m.gelfand@skoltech.ru

Technological advances have led to the creation of large epigenetic datasets, including information about DNA binding proteins and DNA spatial structure. Hi-C experiments have revealed that chromosomes are subdivided into sets of self-interacting domains called Topologically Associating Domains (TADs). TADs are involved in the regulation of gene expression activity, but the mechanisms of their formation are not yet fully understood. Here, we focus on machine learning methods to characterize DNA folding patterns in *Drosophila* based on chromatin marks across three cell lines. We present linear regression models with four types of regularization, gradient boosting, and recurrent neural networks (RNN) as tools to study chromatin folding characteristics associated with TADs given epigenetic chromatin immunoprecipitation data. The bidirectional long short-term memory RNN architecture produced the best prediction scores and identified biologically relevant features. Distribution of protein Chriz (Chromator) and histone modification H3K4me3 were selected as the most informative features for the prediction of TADs characteristics. This approach may be adapted to any similar biological dataset of chromatin features across various cell lines and species. The code for the implemented pipeline, Hi-ChIP-ML, is publicly available: <https://github.com/MichalRozenwald/Hi-ChIP-ML>

A machine learning framework for the prediction of chromatin folding in *Drosophila* using epigenetic features

Michal B. Rozenwald¹, Aleksandra A. Galitsyna², Grigory V. Sapunov^{1,4}, Ekaterina E. Khrameeva², and Mikhail S. Gelfand^{2,3}

¹Faculty of Computer Science, National Research University Higher School of Economics, Moscow, Russia

²Center of Life Sciences, Skolkovo Institute of Science and Technology, Moscow, Russia

³A.A. Kharkevich Institute for Information Transmission Problems, RAS, Moscow, Russia

⁴Intento, Inc, Berkeley, CA, USA

Corresponding author:

Mikhail Gelfand, Michal Rozenwald

Email address: m.gelfand@skoltech.ru, michal.rozenwald@gmail.com

ABSTRACT

Technological advances have led to the creation of large epigenetic datasets, including information about DNA binding proteins and DNA spatial structure. Hi-C experiments have revealed that chromosomes are subdivided into sets of self-interacting domains called Topologically Associating Domains (TADs). TADs are involved in the regulation of gene expression activity, but the mechanisms of their formation are not yet fully understood. Here, we focus on machine learning methods to characterize DNA folding patterns in *Drosophila* based on chromatin marks across three cell lines. We present linear regression models with four types of regularization, gradient boosting, and recurrent neural networks (RNN) as tools to study chromatin folding characteristics associated with TADs given epigenetic chromatin immunoprecipitation data. The bidirectional long short-term memory RNN architecture produced the best prediction scores and identified biologically relevant features. Distribution of protein Chriz (Chromator) and histone modification H3K4me3 were selected as the most informative features for the prediction of TADs characteristics. This approach may be adapted to any similar biological dataset of chromatin features across various cell lines and species. The code for the implemented pipeline, Hi-ChIP-ML, is publicly available: <https://github.com/MichalRozenwald/Hi-ChIP-ML>

INTRODUCTION

Machine learning has proved to be an essential tool for studies in the molecular biology of the eukaryotic cell, in particular, the process of gene regulation (Eraslan et al., 2019; Zeng et al., 2020). Gene regulation of higher eukaryotes is orchestrated by two primary interconnected mechanisms, the binding of regulatory factors to the promoters and enhancers, and the changes in DNA spatial folding. The resulting binding patterns and chromatin structure represent the epigenetic state of the cells. They can be assayed by high-throughput techniques, such as chromatin immunoprecipitation (Ren et al., 2000; Johnson et al., 2007) and Hi-C (Lieberman-Aiden et al., 2009). The epigenetic state is tightly connected with inheritance and disease (Lupiáñez et al., 2016; Yuan et al., 2018; Trieu et al., 2020). For instance, disruption of chromosomal topology in humans affects gliomagenesis and limb malformations (Krijger and De Laat, 2016). However, the details of underlying processes are yet to be understood.

The study of Hi-C maps of genomic interactions revealed the structural and regulatory units of eukaryotic genome, topologically associating domains, or TADs. TADs represent self-interacting regions of DNA with well-defined boundaries that insulate the TAD from interactions with adjacent regions (Lieberman-Aiden et al., 2009; Dixon et al., 2012; Rao et al., 2014). In mammals, the boundaries of TADs

46 are defined by the binding of insulator protein CTCF (Rao et al., 2014). However, *Drosophila* CTCF
47 homolog is not essential for the formation of TAD boundaries (Wang et al., 2018). Contribution of CTCF
48 to the boundaries was detected in neuronal cells, but not in embryonic cells of *Drosophila* (Chathoth and
49 Zabet, 2019). At the same time, up to eight different insulator proteins have been proposed to contribute
50 to the formation of TADs boundaries (Ramírez et al., 2018).

51 Ulianov et al. (2016) demonstrated that active transcription plays a key role in the *Drosophila*
52 chromosome partitioning into TADs. Active chromatin marks are preferably found at TAD borders, while
53 repressive histone modifications are depleted within inter-TADs. Thus, histone modifications instead of
54 insulator binding factors might be the main TAD-forming factors in this organism.

55 To determine factors responsible for the TAD boundary formation in *Drosophila*, Ulianov et al. (2016)
56 utilized machine learning techniques. For that, they formulated a classification task and used a logistic
57 regression model. The model input was a set of ChIP-chip signals for a genomic region, and the output,
58 a binary value indicating whether the region was located at the boundary or within a TAD. Similarly,
59 Ramírez et al. (2018) demonstrated the effectiveness of the lasso regression and gradient boosting for the
60 same task.

61 However, this approach has two substantial limitations. First, the prediction of TAD state as a
62 categorical output depends on the TAD calling procedure. It requires setting a threshold for the TAD
63 boundary definition and it is insensitive to sub-threshold boundaries.

64 Alternatively, the TAD status of a region may be derived from a Hi-C map either by calculation of
65 local characteristics of TADs such as Insulation Score (Crane et al., 2015), D-score (Stadhouders et al.,
66 2018), Directionality Index (Dixon et al., 2012), or by dynamic programming methods, such as Armatus
67 (Filippova et al., 2014). Methods assessing local characteristics of TADs result in assigning a continuous
68 score to genomic bins along the chromosome. Dynamic programming methods are typically not anchored
69 to a local genomic region and consider Hi-C maps of whole chromosomes. The calculation of *transitional*
70 *gamma* has the advantages of both approaches (Ulianov et al., 2016). It runs dynamic programming for
71 whole-chromosome data for multiple parameters and assesses the score for each genomic region.

72 The second limitation is that regression and gradient boosting in Ulianov et al. (2016) and Ramírez
73 et al. (2018) account for the features of a given region of the genome, but ignore the adjacent regions.
74 Such contextual information might be crucial for the TAD status in *Drosophila*.

75 For a possible solution, one may look at instructive examples of other chromatin architecture problems,
76 such as improvement of Hi-C data resolution (Gong et al., 2018; Schwessinger et al., 2019; Li and Dai,
77 2020), inference of chromatin structure (Cristescu et al., 2018; Trieu et al., 2020), prediction of genomic
78 regions interactions (Whalen et al., 2016; Zeng et al., 2018; Li et al., 2019; Fudenberg et al., 2019; Singh
79 et al., 2019; Jing et al., 2019; Gan et al., 2019a; Belokopytova et al., 2020), and, finally, TAD boundaries
80 prediction in mammalian cells (Gan et al., 2019b; Martens et al., 2020).

81 The machine learning approaches used in these works include generalized linear models (Ibn-Salem
82 and Andrade-Navarro, 2019), random forest (Bkhetan and Plewczynski, 2018; Gan et al., 2019b), other
83 ensemble models (Whalen et al., 2016), and neural networks: multi-layer perceptron (Gan et al., 2019b),
84 dense neural networks (Zeng et al., 2018; Farré et al., 2018; Li et al., 2019), convolutional neural
85 networks (Schreiber et al., 2017), generative adversarial networks (Liu et al., 2019), and recurrent neural
86 networks (Cristescu et al., 2018; Singh et al., 2019; Gan et al., 2019a).

87 Among these methods, recurrent neural networks (RNNs) provide a comprehensive architecture for
88 analyzing sequential data (Graves et al., 2013), due to the temporal modeling capabilities. A popular
89 implementation of RNN Long Short-Term Memory (LSTM) models (Hochreiter and Schmidhuber, 1997)
90 create informative statistics that provide solutions for complex long-time-lag tasks (Graves, 2012). Thus,
91 the application of LTSM RNNs to problems with sequential ordering of a target, such as DNA bins
92 characteristics, is a promising approach. Moreover, this feature is particularly relevant for the TAD
93 boundary prediction in *Drosophila*, where the histone modifications of extended genomic regions govern
94 the formation of boundaries (Ulianov et al., 2016).

95 Here, we analyze the epigenetic factors contributing to the TAD status of the genomic regions of
96 *Drosophila*. As opposed to previous approaches, we incorporate information about the region context on
97 two levels. First, we utilize the context-aware TAD characteristic *transitional gamma*. Second, we use the
98 advanced method of recurrent neural network that preserves the information about features of adjacent
99 regions.

100 MATERIALS AND METHODS

101 **Data**

102 Hi-C datasets for three cultured *Drosophila melanogaster* cell lines were taken from Ulianov et al. (2016).
103 Cell lines Schneider-2 (S2) and Kc167 from late embryos and DmBG3-c2 (BG3) from the central nervous
104 system of third-instar larvae were analysed. The *Drosophila* genome (dm3 assembly) was binned at the
105 20-kb resolution resulting in 5950 sequential genomic regions of equal size. Each bin was described
106 by the start coordinate on the chromosome and by the signal from a set of ChIP-chip experiments. The
107 ChIP-chip data were obtained from the modENCODE database (Waterston et al., 2009) and processed as
108 in Ulianov et al. (2016).

109 As chromatin architecture is known to be correlated with epigenetic characteristics in *Drosophila*
110 (Ulianov et al., 2016; Hug et al., 2017; Ramírez et al., 2018), we selected two sets of epigenetic marks,
111 i.e., transcription factors (TF), and insulator protein binding sites, and histone modifications (HM), for
112 further analysis. The first set included five features (Chriz, CTCF, Su(Hw), H3K27me3, H3K27ac), which
113 had been reported as relevant for TAD formation in previous studies (Ulianov et al., 2016). The second set
114 contained eighteen epigenetic marks in total, extending the first set with thirteen potentially relevant fea-
115 tures chosen based on the literature (RNA polymerase II, BEAF-32, GAF, CP190, H3K4me1, H3K4me2,
116 H3K4me3, H3K9me2, H3K9me3, H3K27me1, H3K36me1, H3K36me3, H4K16ac). To normalize the
117 input data, we subtracted the mean from each value and then scaled it to the unit variance using the
118 preprocessing scale function of the Sklearn Python library (Pedregosa et al., 2011). We standardized
119 each feature independently; the mean and variance were calculated per each feature (chromatin mark)
120 separately across all input objects (bins), see Supplementary Fig. 2. For the full list of chromatin factors
121 and their modENCODE IDs, see Supplementary Table 1.

122 **Target Value**

123 TADs are calculated based on Hi-C interactions matrix. As a result of TAD calling algorithm, TADs
124 are represented as a segmentation of the genome into discrete regions. However, resulting segmentation
125 typically depends on TAD calling parameters. In particular, widely used TAD segmentation software
126 Armatus (Filippova et al., 2014) annotates TADs for a user-defined scaling parameter *gamma*. Gamma
127 determines the average size and the number of TADs produced by Armatus on a given Hi-C map.

128 Following Ulianov et al. (2016), we avoided the problem of selection of single set of parameters
129 for TADs annotation and calculated the local characteristic of TAD formation of the genome, namely,
130 *transitional gamma*. The procedure of calculation of transitional gamma includes the TAD calling for
131 a wide range of reasonable parameters gamma and selection of characteristic gamma for each genomic
132 locus. The procedure is briefly described below.

133 When parameter gamma is fixed, Armatus annotates each genomic bin as a part of a TAD, inter-TAD,
134 or TAD boundary. The higher the gamma value is used in Armatus, the smaller on average the TADs
135 sizes are. We perform the TAD calling with Armatus for a set of parameters and characterize each bin by
136 transitional gamma at which this bin switches from being a part of a TAD to being a part of an inter-TAD
137 or a TAD boundary. We illustrate the TADs annotation and calculation of transitional gamma in Figure 1A.

138 Whole-genome Hi-C maps of *Drosophila* cells were collected from Ulianov et al. (2016) and processed
139 using Armatus with a gamma ranging from 0 to 10 with a step of 0.01. We then calculated the transitional
140 gamma for each bin. The resulting distribution of values can be found in Figure 1B. We note that the
141 value 10 is corresponding to the bins that form TAD regions that we have never observed as being TAD
142 boundary or inter-TAD. These bins might switch from TADs with the further increase of gamma. However,
143 they represent a minor fraction of the genome corresponding to strong inner-TAD bins.

144 **Problem statement**

145 To avoid ambiguity, we formally state our machine learning problem:

- 146 • **objects** are genomic bins of 20-kb length that do not intersect,
- 147 • **input features** are the measurements of chromatin factors binding,
- 148 • **target value** is the transitional gamma, which characterizes the TAD status of the region and thus
149 the DNA folding,
- 150 • **objective** is to predict the value of transitional gamma and to identify which of the chromatin
151 features are most significant in predicting the TAD state.

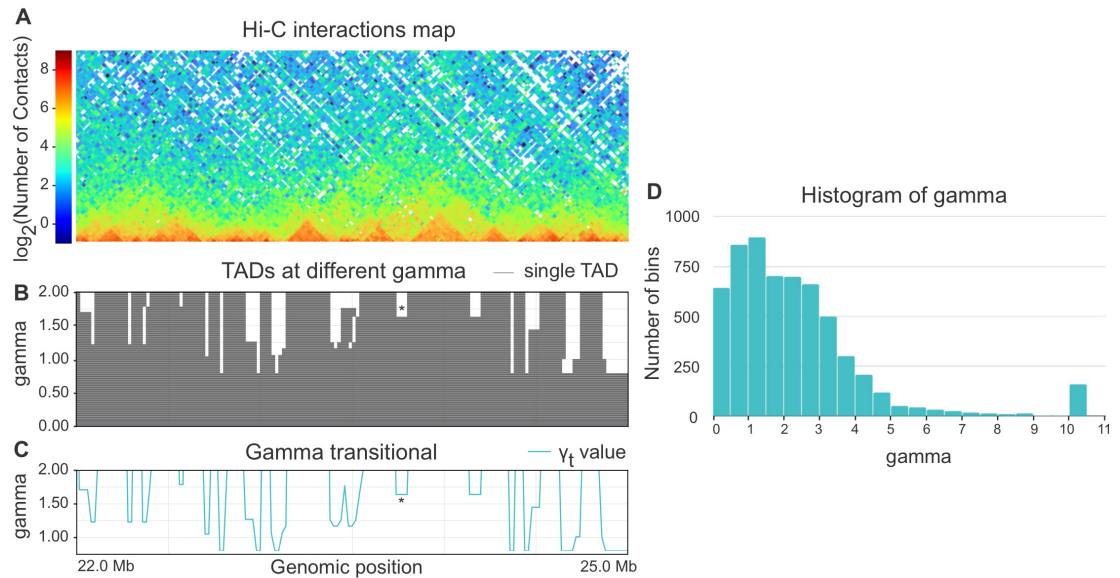


Figure 1. A-C. Example of annotation of chromosome 3R region by gamma transitional. For a given Hi-C matrix of Schneider-2 cells (A), TAD segmentations (B) are calculated by Armatus for a set of gamma values (from 0 to 10, a step of 0.01). Each line in B represents a single TAD. Then gamma transitional (C) is calculated for each genomic region as the minimal value of gamma where the region becomes inter-TAD or TAD boundary. The line in C represents the transitional gamma value for each genomic bin. The plots B and C are limited by gamma 2 for better visualization, although they are continued to the value of 10. Asterisk (*) denotes the region with gamma transitional of 1.64, the minimal value of gamma, where the corresponding region transitions from TAD to inter-TAD. **D.** The histogram of the target value transitional gamma for Schneider-2 cell line. Note the peak at 10.

152 **Selection of Loss Function**

153 The target, transitional gamma, is a continuous variable ranging from 0 to 10, which yields a regression
 154 problem (Yan and Su, 2009). The classical optimization function for the regression is *Mean Square Error*
 155 (*MSE*), instead of precision, recall or accuracy, as for binary variables. However, the distribution of the
 156 target in our problem is significantly unbalanced (see Figure 1D), because the target value of most of the
 157 objects is in the interval between 0 and 3. Thus the contribution of the error on objects with a high true
 158 target value may be also high in the total score when using MSE.

159 We note that the biological nature of genomic bins with high transitional gamma is different from
 160 other bins. Transitional gamma equal to 10 means that the bin never transformed from being a part of
 161 a TAD to an inter-TAD or TAD boundary. To solve this contradiction, we have introduced a custom
 162 loss function called modified *weighted Mean Square Error* (*wMSE*). It might be reformulated as MSE
 163 multiplied by the weight (penalty) of the error, depending on the true value of the target variable.

$$wMSE = \frac{1}{N} \sum_{i=1}^N (y_{\text{true}_i} - y_{\text{pred}_i})^2 \frac{\alpha - y_{\text{true}_i}}{\alpha},$$

164 where N is the number of data points, y_{true_i} is the true value for data point number i , y_{pred_i} is the predicted
 165 value for data point number i . Here, α is the maximum value of y_{true} increased by 1 to avoid multiplying
 166 the error by 0. The maximum value of the transitional gamma in our dataset is 10, thus in our case, α
 167 equals 11. With *wMSE* as a loss function, the model is penalized less for errors on objects with high
 168 values of transitional gamma.

169 **Machine learning models**

170 To explore the relationships between the 3D chromatin structure and epigenetic data, we built linear
 171 regression (LR) models, gradient boosting (GB) regressors, and recurrent neural networks (RNN). The

172 LR models were additionally applied with either L1 or L2 regularization and with both penalties. For
 173 benchmarking we used a constant prediction set to the mean value of the training dataset.

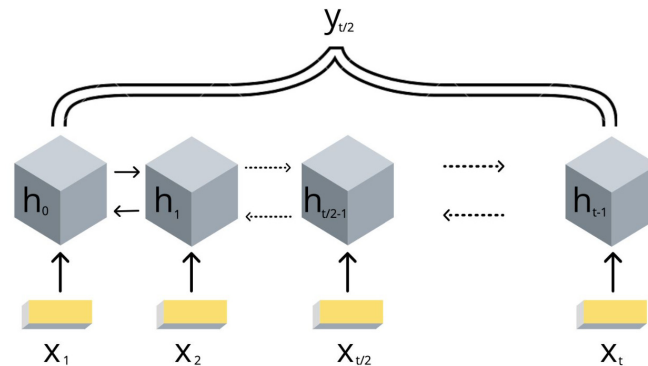


Figure 2. Scheme of the implemented bidirectional LSTM recurrent neural networks with one output. The values of $\{x_1, \dots, x_i\}$ are the DNA bins with input window size t , $\{h_1, \dots, h_i\}$ are the hidden states of the RNN model, $y_{i/2}$ represents the corresponding target value transitional gamma of the middle bin $x_{i/2}$.

173 Due to the DNA linear connectivity, our input bins are sequentially ordered in the genome. Neighbor-
 174 ing DNA regions frequently bear similar epigenetic marks and chromatin properties (Kharchenko et al.,
 175 2011). Thus the target variable values are expected to be vastly correlated. To use this biological property,
 176 we applied RNN models. In addition, the information content of the double-stranded DNA molecule is
 177 equivalent if reading in forward and reverse direction. In order to utilize the DNA linearity together with
 178 equivalence of both direction on DNA, we selected the bidirectional long short-term memory (biLSTM)
 179 RNN architecture (Schuster and Paliwal, 1997). The model takes a set of epigenetic properties for bins as
 180 input and outputs the target value of the *middle bin*. The middle bin is an object from the input set with an
 181 index i , where i equals to the floor division of the input set length by 2. Thus the transitional gamma of
 182 the middle bin is being predicted using the features of the surrounding bins as well. The scheme of this
 183 model is presented in Figure 2.

184 We exploited the following parameters of the biLSTM RNN in our experiments.

185 The sequence length of the RNN input objects is a set of consecutive DNA bins with fixed length that
 186 was varied from 1 to 10 (*window size*).

187 The numbers of LSTM Units that we tested for were 1, 4, 8, 16, 32, 64, 128, 256, 512.

188 The weighted Mean Square Error loss function was chosen and models were trained with a stochastic
 189 optimizer Adam (Kingma and Ba, 2014).

190 Early Stopping was used to automatically identify the optimal number of training epochs.

191 The dataset was randomly split into three groups: train dataset 70%, test dataset 20%, and 10% data for
 192 validation.

193 To explore the importance of each feature from the input space, we trained the RNNs using only one
 194 of the epigenetic features as input. Additionally, we built models in which columns from the feature
 195 matrix were one by one replaced with zeros, and all other features were used for training. Further, we
 196 calculated the evaluation metrics and checked if they were significantly different from the results obtained
 197 while using the complete set of data.

198 RESULTS

199 **Chromatin marks are reliable predictors of the TAD state**

200 First, we assessed whether the TAD state could be predicted from the set of chromatin marks for a single
 201 cell line (Schneider-2 in this section). The classical machine learning quality metrics on cross-validation
 202 averaged over ten rounds of training demonstrate strong quality of prediction compared to the constant
 203 prediction (see Table 1).

204 High evaluation scores prove that the selected chromatin marks represent a set of reliable predictors
 205 for the TAD state of *Drosophila* genomic region. Thus, the selected set of 18 chromatin marks can be
 206 used for chromatin folding patterns prediction in *Drosophila*.

208 The quality metric adapted for our particular machine learning problem, wMSE, demonstrates the
 209 same level of improvement of predictions for different models (see Table 2). Therefore, we conclude that
 210 wMSE can be used for downstream assessment of the quality of the predictions of our models.

211 These results allow us to perform the parameter selection for linear regression (LR) and gradient
 212 boosting (GB) and select the optimal values based on the wMSE metric. For LR, we selected alpha of 0.2
 213 for both L1 and L2 regularizations.

214 Gradient boosting outperforms linear regression with different types of regularization on our task.
 215 Thus, the TAD state of the cell is likely to be more complicated than a linear combination of chromatin
 216 marks bound in the genomic locus. We used a wide range of variable parameters such as the number of
 217 estimators, learning rate, maximum depth of the individual regression estimators. The best results were
 218 observed while setting the 'n_estimators': 100, 'max_depth': 3 and n_estimators': 250, 'max_depth': 4,
 219 both with 'learning_rate': 0.01. The scores are presented in Tables 1 and 2.

220 **The context-aware prediction of TAD state is the most reliable**

221 The alternative model that we studied was biLSTM neural network, which provides explicit accounting
 222 for linearly ordered bins in the DNA molecule.

223 We have investigated the hyperparameters set for biLSTM and assessed the wMSE on various input
 224 window sizes and numbers of LSTM Units. As we demonstrate in Figure 3, the optimal sequence length is
 225 equal to the input window size 6 and 64 LSTM Units. This result has a potential biological interpretation
 226 as the typical size of TADs in *Drosophila*, being around 120 kb at 20-kb resolution Hi-C maps which
 227 equals to 6 bins.

228 The incorporation of sequential dependency improved the prediction significantly, as demonstrated
 229 by the best quality scores achieved by the biLSTM (Table 2). The selected biLSTM with the best
 230 hyperparameters set performed two times better than the constant prediction and outscored all trained LR
 231 and GB models, see Tables 1 and 2. We note that the proposed biLSTM model does not take into account
 232 the target value of the neighboring regions, both while training and predicting. Our model uses the input
 233 values (chromatin marks) solely for the whole window and target values for the central bin in the window
 234 for training and assessment of validation results. Thus, we conclude that biLSTM was able to capture and
 235 utilize the sequential relationship of the input objects in terms of the physical distance in the DNA.

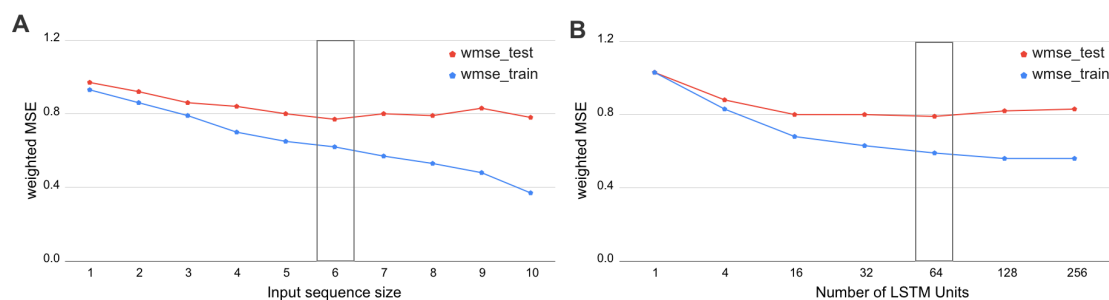


Figure 3. Selection of the biLSTM parameters. Weighted MSE scores for the train and test datasets are presented. **A.** Results of RNN with 64 units for different sizes of sequence length. The sequence size corresponds to the input window size of the RNN or number of bins used together as an input sequence for the neural network. **B.** Results of RNN with an input sequence of 6 bins for the different number of LSTM units. The box highlights the best scores. The biLSTM with 6 input bins and 64 LSTM units was used throughout this study if not specified otherwise.

236 **Reduced set of chromatin marks is sufficient for a reliable prediction of the TAD state in *Drosophila***
 237 Next, we used an opportunity to analyse feature importance and select the set of factors most relevant for
 238 chromatin folding. For an initial analysis, we selected a subset of five chromatin marks that we considered
 239 important based on the literature (two histone marks and three potential insulator proteins, 5-features
 240 model).

241 The 5-features model performed slightly worse than the initial 18-features model (see Tables 1
 242 and 2). The difference in quality scores is rather small, supporting the selection of these five features as
 243 biologically relevant for TAD state prediction.

244 We note that the small impact of shrinking of the number of predictors might indicate the high
 245 correlation between chromatin features. This is in line with the concept of chromatin states when several
 246 histone modifications and other chromatin factors are responsible for a single function of DNA region,
 247 such as gene expression (Filion et al., 2010; Kharchenko et al., 2011).

Table 1. Evaluation of classical machine learning scores for all models, based on 5-features and 18-features inputs

Model type	MSE Train	MSE Test	MAE Train	MAE Test	R^2
Constant prediction	3.71	3.72	1.36	1.31	0
Using 5 features:					
LR + L1	2.91	2.91	1.11	1.11	0.21
LR + L2	2.92	2.93	1.12	1.12	0.21
LR + L1 + L2	2.86	2.87	1.11	1.11	0.23
GB-250	2.45	2.67	1.10	1.11	0.28
biLSTM RNN	2.36	2.90	0.92	1.01	0.33
Using 18 features:					
LR + L1	2.77	2.77	1.09	1.09	0.25
LR + L2	2.69	2.69	1.08	1.08	0.27
LR + L1 + L2	2.67	2.68	1.07	1.07	0.28
GB-250	2.22	2.53	1.06	1.07	0.32
biLSTM RNN	2.03	2.45	0.85	0.90	0.43

Table 2. Weighted MSE of all models, based on 5-features and 18-features inputs

	5 features		18 features	
	Train	Test	Train	Test
Constant prediction	1.61	1.62	1.61	1.62
Linear Regression	1.20	1.20	1.13	1.14
Linear regression + L1	1.17	1.17	1.12	1.12
Linear regression + L2	1.18	1.19	1.11	1.12
Linear regression + L1 + L2	1.17	1.16	1.11	1.11
Grad boosting 100 estimators	1.11	1.13	1.08	1.10
Grad boosting 250 estimators	1.06	1.11	0.95	1.07
biLSTM 64 units & 6 bins	0.83	0.88	0.79	0.84

248 **Feature importance analysis reveals factors relevant for chromatin folding into TADs in *Drosophila***

249 We have evaluated the weight coefficients of the linear regression because the large weights strongly
 250 influence the model prediction. Chromatin marks prioritization of 5-features LR model demonstrated
 251 that the most valuable feature was Chriz, while the weights of Su(Hw) and CTCF were the smallest. As
 252 expected, Chriz factor was the top in the prioritization of the 18-features LR model. However, the next
 253 important features were histone marks H3K4me1 and H3K27me1, supporting the hypothesis of histone
 254 modifications as drivers of TAD folding in *Drosophila*.

255 We used two approaches for the feature selection of RNN: use-one feature and drop-one feature.
 256 When each single chromatin mark was used as the only feature of each bin of the RNN input sequence
 257 for training, the best scores were obtained for Chriz and H3K4me2 (Figure 4, 5 and 6), similarly to the

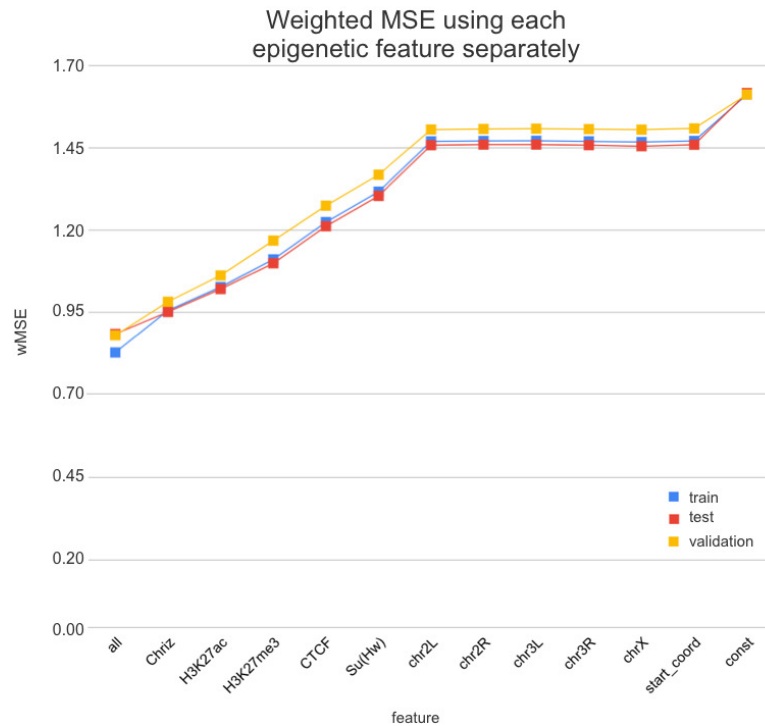


Figure 4. Weighted MSE using one feature for each input bin in the biLSTM RNN. The first mark ('all') corresponds to scores of NNs using the first dataset of chromatin marks features together, the last mark ('const') represents wMSE using constant prediction. Note that the lower the wMSE value the better the quality of prediction.

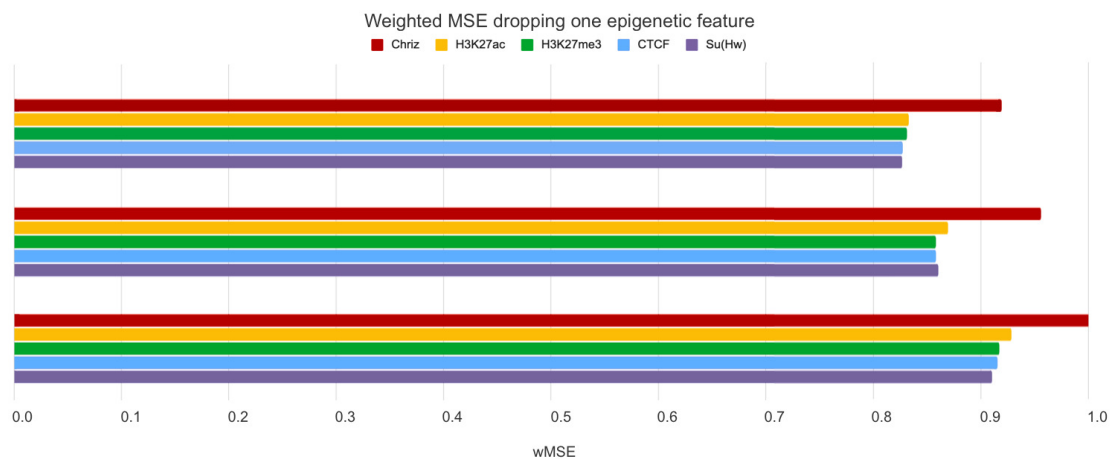


Figure 5. Weighted MSE using four out of five chromatin marks features together as the biLSTM RNN input. Each colour correspond to the feature that was excluded from the input. Note that the model is affected the most when Chr1z factor is dropped from features.

258 LR models results. When we dropped out one of the five features, we got scores that are almost equal
 259 to the wMSE using the full dataset together. This does not hold for experiment with excluded Chr1z,
 260 where wMSE increases. These results align with the outcome of use-one approach and while applying LR
 261 models.

262 Similar results were obtained while using the broader dataset. The results of applying the same

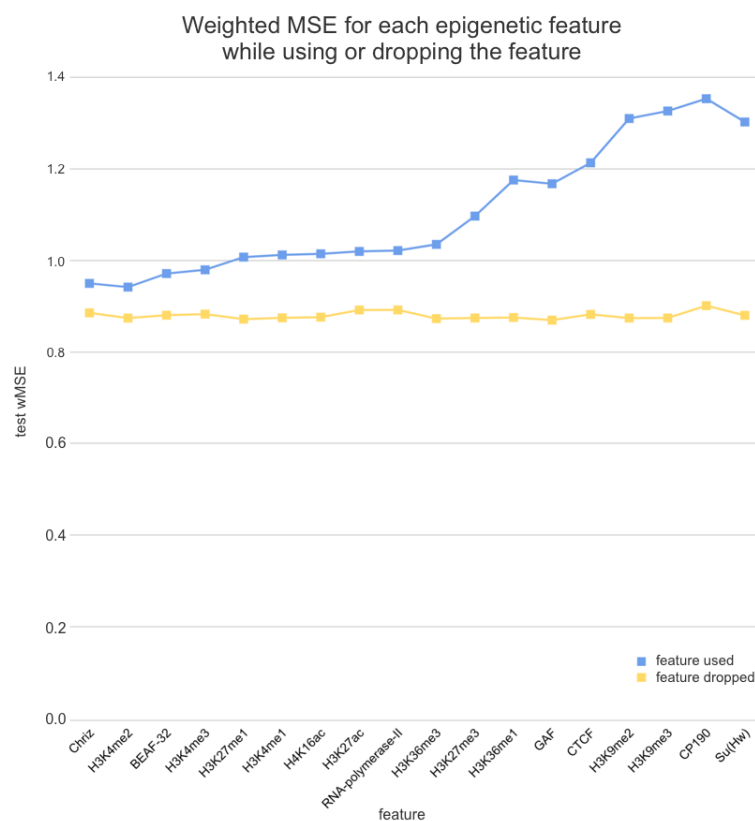


Figure 6. Weighted MSE on the test dataset while using each chromatin mark either as a single feature (blue line) or ejecting it from the biLSTM RNN input (yellow line).

263 approach of omitting each feature one by one using the second dataset of features allowed the evaluation
 264 of the biological impact of the features. The corresponding wMSE scores are presented in Figure 6 as
 265 well as the result of training the model on all features together.

266 The results of omitting each feature one but one while using the second dataset of features are almost
 267 identical as we accepted. It could be explained by the fact that most of the features are strongly correlated.

268 ***TAD state prediction models are transferable between cell lines of Drosophila***

269 In order to explore the transferability of the results between various *Drosophila* cell lines, we have
 270 applied the full pipeline for Schneider-2 and Kc167 from late embryos and DmBG3-c2 (BG3) from the
 271 central nervous system of third-instar larvae. Across all cell lines, the biLSTM model has gained the best
 272 evaluation scores (Table 3). On average, the smallest errors were produced on the test set of the BG3 cell
 273 line.

274 Notably, the selected top features are robust between cell lines. The results of the usage of each
 275 feature separately for each of the cell lines can be found in Supplementary Fig. 1. Chriz was identified
 276 as the most influencing feature for Schneider-2 and BG3 while being in the top four features for Kc167.
 277 Histone modifications H3K4me2 and H3K4me3 gain very high scores on each dataset. However, CTCF
 278 was found in the top of the influencing chromatin marks only on the Kc167. While insulator Su(Hw)
 279 constantly scores almost the worst wMSE across all cell lines.

280 ***The all-cell-lines model improves prediction for most cell lines***

281 Finally, we tested the improvement of the prediction models that can be achieved by merging the
 282 information about all cell lines. For that, we merged all three cell lines as the input dataset and used the
 283 all-cell-lines model for the prediction on each cell line.

284 The gain of scores was the highest for Schneider-2 and Kc167, while BG3 demonstrated a slight
 285 decline in the prediction quality. We also note that biLSTM was less affected by the addition of cross-cell-

Table 3. Weighted MSE on cross-validation of all methods for each cell line and while using them together. Lower wMSE signifies better quality of prediction.

METHOD	SCHNEIDER-2	Kc167	DMBG3-c2	ALL
CONSTANT PREDICTION	1.62 ± 0.09	1.53 ± 0.06	1.36 ± 0.05	1.51 ± 0.04
LINEAR REGRESSION	1.14 ± 0.08	1.01 ± 0.06	0.91 ± 0.08	1.04 ± 0.04
LINEAR REGRESSION + L1	1.12 ± 0.07	1.04 ± 0.06	0.95 ± 0.07	1.05 ± 0.04
LINEAR REGRESSION + L2	1.12 ± 0.07	1.01 ± 0.06	0.9 ± 0.08	1.03 ± 0.04
LINEAR REGRESSION + L1 + L2	1.11 ± 0.07	1.02 ± 0.06	0.91 ± 0.07	1.03 ± 0.04
GRADIENT BOOSTING	1.07 ± 0.06	0.98 ± 0.07	0.86 ± 0.08	0.96 ± 0.04
BILSTM 64 UNITS & 6 BINS	0.86 ± 0.04	0.83 ± 0.04	0.73 ± 0.01	0.78 ± 0.01

286 line data among all models.

287 In general, the quality of the prediction has mostly improved, suggesting the universality of the
288 biological mechanisms of the TAD formation between three cell lines (two embryonic and one neuronal)
289 of *Drosophila*.

290 DISCUSSION

291 Here, we developed the Hi-ChIP-ML framework for the prediction of chromatin folding patterns for a
292 set of input epigenetic characteristics of the genome. Using this framework, we provide the proof of
293 concept that incorporation of information about the context of genomic regions is important for the TAD
294 status and spatial folding of genomic regions. Our approach allows for diverse biological insights into the
295 process of TAD formation in *Drosophila*, identified using the features importance analysis.

296 Firstly, we found that chromodomain protein Chriz, or Chromator (Eggert et al., 2004), might be
297 an important player of the TAD formation mechanism. Recurrent neural networks that used only Chriz
298 as the input produced the highest scores among all RNNs using single epigenetic marks (Figure 5, 7).
299 Moreover, the removal of Chriz, strongly influenced the prediction scores when four out of five selected
300 ChIP features were together (Figure 6). All linear models assigned the highest regression weight to the
301 Chriz input signal. Further, with the L1 regularization Chriz was the only feature that the model selected
302 for prediction. This chromodomain protein is known to be specific for the inter-bands of *Drosophila*
303 *melanogaster* chromosomes (Chepelev et al., 2012), TAD boundaries and the inter-TAD regions (Ulianov
304 et al., 2016), while profiles of proteins that are typically over-represented in inter-bands (including Chriz)
305 correspond to TAD boundaries in embryonic nuclei (Zhimulev et al., 2014). The binding sites of insulator
306 proteins Chriz and BEAF-32 are enriched at TAD boundaries (Hou et al., 2012; Hug et al., 2017; Ramírez
307 et al., 2018; Sexton et al., 2012). Wang et al. (2018) reported the predictor of the boundaries based on
308 the combination of BEAF-32 and Chriz. This might explain BEAF-32 achieving the third rank of the
309 predictability score.

310 Secondly, the application of the recurrent neural network using each of the selected chromatin marks
311 features separately (Fig. 6) has revealed a strong predictive power of active histone modifications such
312 as H3K4me2. This result aligns with the fact that H3K4me2 defines the transcription factor binding
313 regions in different cells, about 90% of transcription factor binding regions (TFBRs) on average overlap
314 with H3K4me2 regions, and use H3K4me2 together with H3K27ac regions to improve the prediction of
315 TFBRs (Wang et al., 2014). Histone modifications H3K4me3, H3K27ac, H3K4me1, H3K4me3, H4K16ac,
316 and other active chromatin marks are also enriched in inter-TADs and TAD boundaries (Ulianov et al.,
317 2016). In addition, H3K27ac and H3K4me1 distinguish poised and active enhancers (Barski et al., 2007;
318 Creyghton et al., 2010; Rada-Iglesias et al., 2011).

319 Thirdly, models using Su(Hw) and CTCF perform as expected given that, the prediction of TAD
320 boundaries, the binding of insulator proteins Su(Hw) and CTCF have performed worse than other
321 chromatin marks (Ulianov et al., 2016). In *Drosophila*, the absence of strong enrichment of CTCF at TAD
322 boundaries and preferential location of Su(Hw) inside TADs implies that CTCF- and Su(Hw)-dependent
323 insulation is not a major determinant of TAD boundaries. Our results also demonstrate that the impact of
324 Su(Hw) and CTCF is low for both proteins.

325 Thus, our framework not only accurately predicts positions of TADs in the genome but also highlights

326 epigenetic features relevant for the TAD formation. Importantly, the use of adjacent DNA bins created a
327 meaningful biological context and enabled the training of a comprehensive ML model, strongly improving
328 the evaluation scores of the best RNN model.

329 We note that there are few limitations to our approach. In particular, the resolution of our analysis is
330 20 kb, while TAD properties and TAD-forming factors can be different at finer resolutions (Wang et al.,
331 2018; Rowley et al., 2017, 2019). On the other hand, the use of coarse models allowed us to test the
332 approach and select the best parameters while training the models multiple times efficiently. The training
333 of the model for Hi-C with the resolution up to 500 bp presents a promising direction for future work,
334 leading to the clarification of other factors' roles in the formation of smaller TAD boundaries that are
335 beyond the resolution of our models.

336 We also note that transitional gamma is just one of multiple measures of the TAD state for a genomic
337 region. We motivate the use of transitional gamma by the fact that it is a parameter-independent way
338 of assessing TAD prominence calculated for the entire map. This guarantees the incorporation of the
339 information about the interactions of the whole chromosome at all genomic ranges, which is not the case
340 for other approaches such as the Insulation Score (Crane et al., 2015), D-score (Stadhouders et al., 2018),
341 and Directionality Index (Dixon et al., 2012). On the other hand, the presented pipeline may be easily
342 transferred to predict these scores as target values, which is an important direction for the extension of the
343 work.

344 Here we selected features that had been reported to be associated with the chromatin structure. We
345 note there might be other factors contributing to the TAD formation that were not included in our analysis.
346 The exploration of a broader set of cell types might be a promising direction for this research, as well as
347 the integration of various biological features, such as raw DNA sequence, to the presented models. We
348 also anticipate promising outcomes of applying our approach to study the chromatin folding in various
349 species except for *Drosophila*.

350 The code is open-source and can be easily adapted to various related tasks.

351 CONCLUSIONS

352 To sum up, we developed an approach for analysis of a set of chromatin marks as predictors of the
353 TAD state for a genomic locus. We demonstrate a strong empirical performance of linear regression,
354 gradient boosting, and recurrent neural network prediction models for several cell lines and a number of
355 chromatin marks. The selected set of chromatin marks can reliably predict the chromatin folding patterns
356 in *Drosophila*.

357 Recurrent neural networks incorporate the information about epigenetic surroundings. The highest
358 prediction scores were obtained by the models with the biologically interpretable input size of 120 kb that
359 aligns with the average TAD size for the 20 kb binning in *Drosophila*. Thus, we propose that the explicit
360 accounting for linearly ordered bins is important for chromatin structure prediction.

361 The top-influencing TAD-forming factors of *Drosophila* are Chr3 and histone modification H3K4me2.
362 The chromatin factors that influence the prediction most are stable across the cell lines, which suggests
363 the universality of the biological mechanisms of TAD formation for two embryonic and one neuronal
364 *Drosophila* cell line. On the other hand, the training of models on all cell lines simultaneously generally
365 improves the prediction.

366 The implemented pipeline called Hi-ChIP-ML is open-source. The methods can be used to explore
367 the 3D chromatin structure of various species and may be adapted to any similar biological problem and
368 dataset. The code is freely available at: <https://github.com/MichalRozenwald/Hi-ChIP-ML>

369 **REFERENCES**

- 370 Barski, A., Cuddapah, S., Cui, K., Roh, T.-Y., Schones, D. E., Wang, Z., Wei, G., Chepelev, I., and Zhao, K.
371 (2007). High-resolution profiling of histone methylations in the human genome. *Cell*, 129(4):823–837.
- 372 Belokopytova, P. S., Nuriddinov, M. A., Mozheiko, E. A., Fishman, D., and Fishman, V. (2020). Quantita-
373 tive prediction of enhancer–promoter interactions. *Genome Research*, 30(1):72–84.
- 374 Bkhetan, Z. A. and Plewczynski, D. (2018). Three-dimensional Epigenome Statistical Model : Genome-
375 wide Chromatin Looping Prediction. *Scientific Reports*, pages 1–11.
- 376 Chathoth, K. T. and Zabet, N. R. (2019). Chromatin architecture reorganization during neuronal cell
377 differentiation in Drosophila genome. *Genome Research*, 29(4):613–625.
- 378 Chepelev, I., Wei, G., Wangsa, D., Tang, Q., and Zhao, K. (2012). Characterization of genome-wide
379 enhancer-promoter interactions reveals co-expression of interacting genes and modes of higher order
380 chromatin organization. *Cell Research*, 22(3):490–503.
- 381 Crane, E., Bian, Q., McCord, R. P., Lajoie, B. R., Wheeler, B. S., Ralston, E. J., Uzawa, S., Dekker, J.,
382 and Meyer, B. J. (2015). Condensin-driven remodelling of x chromosome topology during dosage
383 compensation. *Nature*, 523(7559):240–244.
- 384 Creighton, M. P., Cheng, A. W., Welstead, G. G., Kooistra, T., Carey, B. W., Steine, E. J., Hanna, J.,
385 Lodato, M. A., Frampton, G. M., Sharp, P. A., Boyer, L. A., Young, R. A., and Jaenisch, R. (2010).
386 Histone h3k27ac separates active from poised enhancers and predicts developmental state. *Proceedings*
387 *of the National Academy of Sciences*, 107(50):21931–21936.
- 388 Cristescu, B.-C., Borsos, Z., Lygeros, J., Martínez, M. R., and Rapsomaniki, M. A. (2018). Inference of
389 the three-dimensional chromatin structure and its temporal behavior. *arXiv:1811.09619*.
- 390 Dixon, J. R., Selvaraj, S., Yue, F., Kim, A., Li, Y., Shen, Y., Hu, M., Liu, J. S., and Ren, B. (2012).
391 Topological domains in mammalian genomes identified by analysis of chromatin interactions. *Nature*,
392 485(7398):376–380.
- 393 Eggert, H., Gortchakov, A., and Saumweber, H. (2004). Identification of the drosophila interband-specific
394 protein z4 as a dna-binding zinc-finger protein determining chromosomal structure. *Journal of Cell*
395 *Science*, 117(18):4253–4264.
- 396 Eraslan, G., Avsec, Ž., Gagneur, J., and Theis, F. J. (2019). Deep learning: new computational modelling
397 techniques for genomics. *Nature Reviews Genetics*.
- 398 Farré, P., Heurteau, A., Cuvier, O., and EMBERLY, E. (2018). Dense neural networks for predicting
399 chromatin conformation. *BMC Bioinformatics*, 19(1):1–12.
- 400 Fillion, G. J., van Bommel, J. G., Braunschweig, U., Talhout, W., Kind, J., Ward, L. D., Brugman, W.,
401 de Castro, I. J., Kerkhoven, R. M., Bussemaker, H. J., and van Steensel, B. (2010). Systematic Protein
402 Location Mapping Reveals Five Principal Chromatin Types in Drosophila Cells. *Cell*, 143(2):212–224.
- 403 Filippova, D., Patro, R., Duggal, G., and Kingsford, C. (2014). Identification of alternative topological
404 domains in chromatin. *Algorithms for Molecular Biology*, 9(1):14.
- 405 Fudenberg, G., Kelley, D. R., and Pollard, K. S. (2019). Predicting 3D genome folding from DNA
406 sequence. *bioRxiv*, page 800060.
- 407 Gan, M., Li, W., and Jiang, R. (2019a). EnContact: Predicting enhancer-enhancer contacts using
408 sequence-based deep learning model. *PeerJ*, 2019(9):1–19.
- 409 Gan, W., Luo, J., Li, Y. Z., Guo, J. L., Zhu, M., and Li, M. L. (2019b). A computational method to predict
410 topologically associating domain boundaries combining histone marks and sequence information. *BMC*
411 *genomics*, 20(13):1–12.
- 412 Gong, Y., Lazaris, C., Sakellaropoulos, T., Lozano, A., Kambadur, P., Ntziachristos, P., Aifantis, I., and
413 Tsirigos, A. (2018). Stratification of TAD boundaries reveals preferential insulation of super-enhancers
414 by strong boundaries. *Nature Communications*, 9(1).
- 415 Graves, A. (2012). Supervised sequence labelling. In *Supervised sequence labelling with recurrent neural*
416 *networks*, pages 5–13. Springer.
- 417 Graves, A., Jaitly, N., and Mohamed, A.-r. (2013). Hybrid speech recognition with deep bidirectional lstm.
418 In *2013 IEEE workshop on automatic speech recognition and understanding*, pages 273–278. IEEE.
- 419 Hochreiter, S. and Schmidhuber, J. (1997). Long short-term memory. *Neural computation*, 9(8):1735–
420 1780.
- 421 Hou, C., Li, L., Qin, Z. S., and Corces, V. G. (2012). Gene density, transcription, and insulators contribute
422 to the partition of the drosophila genome into physical domains. *Molecular Cell*, 48(3):471–484.
- 423 Hug, C. B., Grimaldi, A. G., Kruse, K., and Vaquerizas, J. M. (2017). Chromatin architecture emerges

- during zygotic genome activation independent of transcription. *Cell*, 169(2):216–228.
- 425 Ibn-Salem, J. and Andrade-Navarro, M. A. (2019). 7C: Computational Chromosome Conformation
426 Capture by Correlation of ChIP-seq at CTCF motifs. *BMC Genomics*, 20(1).
- 427 Jing, F., Zhang, S., Cao, Z., and Zhang, S. (2019). An integrative framework for combining sequence
428 and epigenomic data to predict transcription factor binding sites using deep learning. *IEEE/ACM
429 transactions on computational biology and bioinformatics*.
- 430 Johnson, D. S., Mortazavi, A., Myers, R. M., and Wold, B. (2007). Genome-wide mapping of in vivo
431 protein-dna interactions. *Science*, 316(5830):1497–1502.
- 432 Kharchenko, P. V., Alekseyenko, A. A., Schwartz, Y. B., Minoda, A., Riddle, N. C., Ernst, J., Sabo, P. J.,
433 Larschan, E., Gorchakov, A. A., Gu, T., Linder-Basso, D., Plachetka, A., Shanower, G., Tolstorukov,
434 M. Y., Luquette, L. J., Xi, R., Jung, Y. L., Park, R. W., Bishop, E. P., Canfield, T. K., Sandstrom, R.,
435 Thurman, R. E., MacAlpine, D. M., Stamatoyannopoulos, J. A., Kellis, M., Elgin, S. C. R., Kuroda,
436 M. I., Pirrotta, V., Karpen, G. H., and Park, P. J. (2011). Comprehensive analysis of the chromatin
437 landscape in *drosophila melanogaster*. *Nature*, 471(7339):480–485.
- 438 Kingma, D. P. and Ba, J. (2014). Adam: A method for stochastic optimization. *arXiv preprint
439 arXiv:1412.6980*.
- 440 Krijger, P. H. L. and De Laat, W. (2016). Regulation of disease-associated gene expression in the 3d
441 genome. *Nature Reviews Molecular Cell Biology*, 17(12):771–782.
- 442 Li, W., Wong, W. H., and Jiang, R. (2019). DeepTACT: Predicting 3D chromatin contacts via bootstrapping
443 deep learning. *Nucleic Acids Research*, 47(10):1–14.
- 444 Li, Z. and Dai, Z. (2020). Srhic: A deep learning model to enhance the resolution of hi-c data. *Frontiers
445 in Genetics*, 11:353.
- 446 Lieberman-Aiden, E., van Berkum, N. L., Williams, L., Imakaev, M., Ragoczy, T., Telling, A., Amit, I.,
447 Lajoie, B. R., Sabo, P. J., Dorschner, M. O., Sandstrom, R., Bernstein, B., Bender, M. A., Groudine,
448 M., Gnirke, A., Stamatoyannopoulos, J., Mirny, L. A., Lander, E. S., and Dekker, J. (2009). Compre-
449 hensive mapping of long-range interactions reveals folding principles of the human genome. *Science*,
450 326(5950):289–293.
- 451 Liu, Q., Lv, H., and Jiang, R. (2019). hicgan infers super resolution hi-c data with generative adversarial
452 networks. *Bioinformatics*, 35(14):i99–i107.
- 453 Lupiáñez, D. G., Spielmann, M., and Mundlos, S. (2016). Breaking tads: how alterations of chromatin
454 domains result in disease. *Trends in Genetics*, 32(4):225–237.
- 455 Martens, L. D., Faust, O., Pirvan, L., Bihary, D., and Samarajiwa, S. A. (2020). Identifying regulatory and
456 spatial genomic architectural elements using cell type independent machine and deep learning models.
457 *bioRxiv*.
- 458 Pedregosa, F., Varoquaux, G., Gramfort, A., Michel, V., Thirion, B., Grisel, O., Blondel, M., Prettenhofer,
459 P., Weiss, R., Dubourg, V., Vanderplas, J., Passos, A., Cournapeau, D., Brucher, M., Perrot, M., and
460 Duchesnay, E. (2011). Scikit-learn: Machine learning in Python. *Journal of Machine Learning
461 Research*, 12:2825–2830.
- 462 Rada-Iglesias, A., Bajpai, R., Swigut, T., Brugmann, S. A., Flynn, R. A., and Wysocka, J. (2011). A unique
463 chromatin signature uncovers early developmental enhancers in humans. *Nature*, 470(7333):279–283.
- 464 Ramírez, F., Bhardwaj, V., Arrigoni, L., Lam, K. C., Grüning, B. A., Villaveces, J., Habermann, B.,
465 Akhtar, A., and Manke, T. (2018). High-resolution tads reveal dna sequences underlying genome
466 organization in flies. *Nature communications*, 9(1):1–15.
- 467 Rao, S. S. P., Huntley, M. H., Durand, N. C., Stamenova, E. K., Bochkov, I. D., Robinson, J. T., Sanborn,
468 A. L., Machol, I., Omer, A. D., Lander, E. S., and Aiden, E. L. (2014). A 3D map of the human genome
469 at kilobase resolution reveals principles of chromatin looping. *Cell*, 159(7):1665–1680.
- 470 Ren, B., Robert, F., Wyrick, J. J., Aparicio, O., Jennings, E. G., Simon, I., Zeitlinger, J., Schreiber, J.,
471 Hannett, N., Kanin, E., Volkert, T. L., Wilson, C. J., Bell, S. P., and Young, R. A. (2000). Genome-wide
472 location and function of DNA binding proteins. *Science*, 290(5500):2306–2309.
- 473 Rowley, M. J., Lyu, X., Rana, V., Ando-Kuri, M., Karns, R., Bosco, G., and Corces, V. G. (2019).
474 Condensin II Counteracts Cohesin and RNA Polymerase II in the Establishment of 3D Chromatin
475 Organization. *Cell Reports*, 26(11):2890–2903.e3.
- 476 Rowley, M. J., Nichols, M. H., Lyu, X., Ando-Kuri, M., Rivera, I. S. M., Hermetz, K., Wang, P., Ruan, Y.,
477 and Corces, V. G. (2017). Evolutionarily Conserved Principles Predict 3D Chromatin Organization.
478 *Molecular Cell*, 67(5):837–852.e7.

- 479 Schreiber, J., Libbrecht, M., Bilmes, J., and Noble, W. S. (2017). Nucleotide sequence and DNaseI
480 sensitivity are predictive of 3D chromatin architecture. *bioRxiv*, page 14.
- 481 Schuster, M. and Paliwal, K. (1997). Bidirectional recurrent neural networks. *IEEE Transactions on*
482 *Signal Processing*, 45(11):2673–2681.
- 483 Schwesinger, R., Gosden, M., Downes, D., Brown, R., Telenius, J., Teh, Y. W., Lunter, G., and Hughes,
484 J. R. (2019). DeepC: Predicting chromatin interactions using megabase scaled deep neural networks
485 and transfer learning. *bioRxiv*, page 724005.
- 486 Sexton, T., Yaffe, E., Kenigsberg, E., Bantignies, F., Leblanc, B., Hoichman, M., Parrinello, H., Tanay,
487 A., and Cavalli, G. (2012). Three-dimensional folding and functional organization principles of the
488 drosophila genome. *Cell*, 148(3):458–472.
- 489 Singh, S., Yang, Y., Poczos, B., and Ma, J. (2019). Predicting enhancer-promoter interaction from
490 genomic sequence with deep neural networks. *Quantitative Biology*, 7(2):122–137.
- 491 Stadhouders, R., Vidal, E., Serra, F., Di Stefano, B., Le Dily, F., Quilez, J., Gomez, A., Collombet,
492 S., Berenguer, C., Cuartero, Y., Hecht, J., Filion, G. J., Beato, M., Marti-Renom, M. A., and Graf,
493 T. (2018). Transcription factors orchestrate dynamic interplay between genome topology and gene
494 regulation during cell reprogramming. *Nature Genetics*, 50(2):238–249.
- 495 Trieu, T., Martinez-Fundichely, A., and Khurana, E. (2020). Deepmilo: a deep learning approach to
496 predict the impact of non-coding sequence variants on 3d chromatin structure. *Genome biology*,
497 21(1):1–11.
- 498 Ulianov, S. V., Khrameeva, E. E., Gavrillov, A. A., Flyamer, I. M., Kos, P., Mikhaleva, E. A., Penin,
499 A. A., Logacheva, M. D., Imakaev, M. V., Chertovich, A., Gelfand, M. S., Shevelyov, Y. Y., and Razin,
500 S. V. (2016). Active chromatin and transcription play a key role in chromosome partitioning into
501 topologically associating domains. *Genome research*, 26(1):70–84.
- 502 Wang, Q., Sun, Q., Czajkowsky, D. M., and Shao, Z. (2018). Sub-kb hi-c in d. melanogaster reveals
503 conserved characteristics of tads between insect and mammalian cells. *Nature Communications*,
504 9(1):1–8.
- 505 Wang, Y., Li, X., and Hu, H. (2014). H3k4me2 reliably defines transcription factor binding regions in
506 different cells. *Genomics*, 103(2):222–228.
- 507 Waterston, R., Celniker, S., Snyder, M., White, K., Henikoff, S., and Karpen, G. (2009). Unlocking the
508 secrets of the genome. *Nature*, 459(7249):927–930.
- 509 Whalen, S., Truty, R. M., and Pollard, K. S. (2016). Enhancer–promoter interactions are encoded by
510 complex genomic signatures on looping chromatin. *Nature genetics*, 48(5):488–496.
- 511 Yan, X. and Su, X. (2009). *Linear regression analysis: theory and computing*. World Scientific.
- 512 Yuan, Y., Shi, Y., Su, X., Zou, X., Luo, Q., Feng, D. D., Cai, W., and Han, Z.-G. (2018). Cancer type
513 prediction based on copy number aberration and chromatin 3d structure with convolutional neural
514 networks. *BMC genomics*, 19(6):565.
- 515 Zeng, W., Wang, Y., and Jiang, R. (2020). Integrating distal and proximal information to predict gene
516 expression via a densely connected convolutional neural network. *Bioinformatics*, 36(2):496–503.
- 517 Zeng, W., Wu, M., and Jiang, R. (2018). Prediction of enhancer-promoter interactions via natural language
518 processing. *BMC Genomics*, 19(Suppl 2).
- 519 Zhimulev, I. F., Zykova, T. Y., Goncharov, F. P., Khoroshko, V. A., Demakova, O. V., Semeshin, V. F.,
520 Pokholkova, G. V., Boldyreva, L. V., Demidova, D. S., Babenko, V. N., Demakov, S. A., and Belyaeva,
521 E. S. (2014). Genetic organization of interphase chromosome bands and interbands in drosophila
522 melanogaster. *PLOS ONE*, 9(7):1–16.